Chinese Journal of Natural Medicines

Data mining and multi-omics profiling to reveal the mechanisms of cold/hot property of traditional Chinese medicine in Alzheimer's disease treatment

Mingtao Zhu, Yu Wang, Haipeng Tang, Yanping Sun, Xiaotao Feng, Qiuhong Wang, Haixue Kuang

Citation: Mingtao Zhu, Yu Wang, Haipeng Tang, Yanping Sun, Xiaotao Feng, Qiuhong Wang, Haixue Kuang, Data mining and multi-omics profiling to reveal the mechanisms of cold/hot property of traditional Chinese medicine in Alzheimer's disease treatment, Chinese Journal of Natural Medicines, 2026, 24(10), 1221-1236. doi: 10.1016/S1875-5364(26)61216-2.

View online: https://doi.org/10.1016/S1875-5364(26)61216-2

Related articles that may interest you

Network pharmacology approaches for research of Traditional Chinese Medicines
Chinese Journal of Natural Medicines. 2023, 21(5), 323-332 https://doi.org/10.1016/S1875-5364(23)60429-7

Probiotics with anti-type 2 diabetes mellitus properties: targets of polysaccharides from traditional Chinese medicine
Chinese Journal of Natural Medicines. 2022, 20(9), 641-655 https://doi.org/10.1016/S1875-5364(22)60210-3

Traditional Chinese medicine-based drug delivery systems for anti-tumor therapies
Chinese Journal of Natural Medicines. 2024, 22(12), 1177-1192 https://doi.org/10.1016/S1875-5364(24)60746-6

Therapeutic potential and mechanism of Chinese herbal medicines in treating fibrotic liver disease
Chinese Journal of Natural Medicines. 2023, 21(9), 643-657 https://doi.org/10.1016/S1875-5364(23)60443-1

Effects of traditional Chinese medicine on treatment outcomes in severe COVID-19 patients: a single-centre study
Chinese Journal of Natural Medicines. 2024, 22(1), 89-96 https://doi.org/10.1016/S1875-5364(24)60565-0

Traditional Chinese medicines derived natural inhibitors of ferroptosis on ischemic stroke
Chinese Journal of Natural Medicines. 2024, 22(8), 746-755 https://doi.org/10.1016/S1875-5364(24)60603-5

Wechat

Chinese Journal of Natural Medicines 24 (2026) 1221-1236

Contents lists available at ScienceDirect

Chinese Journal of Natural Medicines

journal homepage: www.cjnmcpu.com/



Original article

Data mining and multi-omics profiling to reveal the mechanisms of cold/hot property of traditional Chinese medicine in Alzheimer's disease treatment

Mingtao Zhu[a], Yu Wang[b], Haipeng Tang[b], Yanping Sun[b], Xiaotao Feng[b], Qiuhong Wang[c,*], Haixue Kuang[b,*]

[a] College of Traditional Chinese Medicine, Wenzhou Medical University, Wenzhou 325035, China
[b] Key Laboratory of Basic and Application Research of Beiyao (Heilongjiang University of Chinese Medicine), Ministry of Education, Harbin 150040, China
[c] School of Traditional Chinese Medicine, Guangdong Pharmaceutical University, Guangzhou 510024, China

ARTICLE INFO

Article history:
Received 12 April 2026
Revised 23 July 2026
Accepted 28 July 2026
Available online 20 October 2026

Keywords:
Alzheimer's disease
Data mining
Multi-omics
Medicinal property
Traditional Chinese medicine

ABSTRACT

Alzheimer's disease (AD) is a severely debilitating condition that significantly hampers independent living, with no effective treatments currently available. Traditional Chinese medicine (TCM) has shown substantial promise in both preventing and alleviating AD symptoms. The medicinal properties—specifically hot, warm, cool, and cold—serve as a critical link between TCM theory and clinical application. However, the majority of research has concentrated on individual herbs for AD, with relatively few comprehensive studies exploring the biological mechanisms through which these herbs exert their medicinal properties. In this context, data mining, network pharmacology, and multi-omics approaches, including metabolomics, gut microbiota analysis, and proteomics, were employed to elucidate the effects and mechanisms of action of three hot/warm property herbs (THPH) and three cold/cool property herbs (TCPH) in the treatment of AD. Findings indicated that the herbs effective against AD primarily possess warm properties. THPH demonstrated a significant enhancement in cognitive, learning, and memory functions in AD rat models when compared to TCPH, potentially achieving therapeutic effects by boosting the synthesis of the neurotransmitter acetylcholine. Furthermore, THPH modulated energy metabolism, corrected metabolic imbalances in both brain and serum within AD rat models, inhibited oxidative stress, restored synaptic plasticity-related proteins and signaling pathways, and maintained intestinal microbiota homeostasis. Consequently, this study offers valuable insights into the therapeutic implications of the hot (warm) and cold (cool) properties of TCM in the management of Alzheimer's disease.

1. Introduction

The ongoing modernization of Traditional Chinese Medicine (TCM) research continually reveals the scientific foundations underlying TCM theories and clinical practices. Central to this exploration is the concept of "medicinal property", including classifications such as hot, warm, cool, and cold, which serve as a vital connection between TCM theory and its clinical applications. These properties are believed to elicit specific physiological responses that are utilized in the treatment of various diseases [1]. For instance, *Coptis chinensis* Franch. has demonstrated the ability to alleviate thirst in diabetic patients, a symptom frequently associated with fever [2]. Bacillary dysentery, a classic representation of heat syndrome (fever) in TCM, shows a favorable response to cold-natured herbs such as *Rheum officinale*, *Phellodendron chinense*, and *Coptis chinensis* Franch [3]. Furthermore, cold-natured herbs like *Scutellaria baicalensis* Georgi, *Coptis chinensis* Franch., *Gardenia jasminoides* J.Ellis, and *Rheum palmatum* L. have proven effective in alleviating hyperthyroidism, a condition categorized as heat syndrome. Their mechanisms of action include the inhibition of energy metabolism, suppression of thyroid hormone synthesis, and the exertion of anti-inflammatory and antioxidant effects [4]. In contrast, hot-natured herbs such as *Aconitum carmichaelii* Debx., *Zingiber officinale* Rosc., *Cinnamomum cassia* Presl, and *Euodia rutaecarpa* (Juss.) Benth. have been shown to enhance hypothyroidism (cold syndrome) by stimulating energy metabolism and increasing thyroid hormone levels [1].

To date, no reports have explored the effects of hot (warm) and cold (cool) properties of TCM on Alzheimer's disease (AD). AD is a chronic central nervous system (CNS) syndrome predominantly affecting the elderly, clinically characterized by the progressive deterioration of cognitive function and memory [5]. In AD, neuronal energy metabolism is impaired, leading to a reduction in overall metabolic capacity [6]. Furthermore, the cholinergic system—essential for brain homeostasis, plasticity, and learning/memory functions—becomes disrupted, with abnormally elevated acetylcholinesterase (AChE) activity [7]. Herbal properties influence the body's energy metabolism through various pathways [8]. Hot (warm) TCMs can elevate the basal metabolic rate and stimulate the CNS, while cold (cool) TCMs appear to reverse this process [9]. Prior studies conducted by our research group revealed that hot (warm) TCMs inhibit AChE activity, whereas cold (cool) TCMs exhibit the opposite effect. Based on key risk factors

* Corresponding author.
E-mail addresses: qhwang@hljucm.net (Q. Wang); hxkuang15@hotmail.com (H. Kuang)

https://doi.org/10.1016/S1875-5364(26)61216-2
Copyright © 2026, China Pharmaceutical University. Published by Elsevier B.V. All rights are reserved.

for AD and the biological effect patterns identified in earlier work, it is reasonable to speculate that the hot (warm) properties of TCM may exert more therapeutic effects on AD than the cold (cool) properties. Additionally, TCM theory commonly associates AD with kidney deficiency and marrow depletion, phlegm turbidity, and blood stasis. However, the theoretical alignment of these pathological mechanisms with the therapeutic effects of "warm/hot" medicinal properties—such as tonification, warming unblocking, and cold dispersing—remains unclear.

Data mining offers a level of scientific rigor that facilitates the rapid screening and extraction of complex, multidimensional TCM data across various levels and dimensions [10]. This capability renders TCM information more intuitive, thus enhancing the reliability of clinical diagnoses and the development of new drugs. Metabolomics, 16S rDNA sequencing, and proteomics capture alterations in metabolism, gut microbiota, and proteins within the body. Their holistic focus aligns well with TCM's comprehensive effects, making these tools particularly suitable for studying medicinal properties. To validate the aforementioned hypothesis, an experimental protocol was designed for this study. Initially, data mining methods were employed to investigate medication patterns of TCM treatments for AD. Subsequently, three hot/warm property herbs (THPH) and three cold/cool property herbs (TCPH), not clinically utilized for AD (to focus on the pure regulatory effects of medicinal properties themselves and minimize the confounding effects of inherent anti-AD components and clinical application experience associated with commonly used anti-AD herbs), were selected. Network pharmacology was utilized to explore the potential targets of THPH and TCPH for AD. A multidimensional evaluation strategy was then applied to comprehensively analyze their effects on AD, focusing on changes in risk factors, endogenous metabolites, differential protein levels, and gut microbiota composition and relative abundance, along with their interconnections. The findings from this study aim to provide valuable insights into the clinical application of TCM property theories and support the development of targeted therapeutic strategies for AD.

2. Materials and methods

2.1. Literature data mining

A comprehensive literature search was conducted across both Chinese (CNKI, VIP, Wan Fang Database) and English (PubMed, ScienceDirect) databases utilizing combinatorial search terms, inclusion criteria, and exclusion criteria. The publication timeline spanned from January 2000 to December 2025. Following the removal of duplicates and standardization of herb names, the analysis focused on the frequency of use, characteristics, and meridian classifications of potential herbs. Additionally, core herb combinations were established. Detailed methods and bibliographic references are provided in the supplementary materials (Supplementary File 1: Methods).

2.2. Network pharmacology target prediction

Active ingredients from THPH and TCPH herbal categories were screened from drug databases based on parameters of oral bioavailability (OB ≥ 30%) and drug-likeness (DL ≥ 0.18). Potential biological targets for these ingredients were predicted using TCMSP, SwissTargetPrediction, and PharmMapper, with standard gene symbols obtained *via* UniProt. AD-related genes were gathered from OMIM, DrugBank, TTD, and GeneCards. Common targets among THPH, TCPH, and AD were identified by intersecting compound-related and disease-related genes. Shared targets were analyzed using STRING to construct protein-protein interaction (PPI) networks, and compound-target networks were visualized using Cytoscape 3.7.2. Gene Ontology (GO) and Kyoto Encyclopedia of Genes and Genomes (KEGG) enrichment analyses were carried out through Metascape.

2.3. Chemicals and reagents

The three warm TCMs—*Arisaema heterophyllum* Blume. (TNX, batch number: 20230316), *Curcuma longa* L. (JH, batch number: 20230911), and *Allium macrostemon* Bunge. (XB, batch number: 20231010)—were sourced alongside the three cold TCMs—*Curcuma aromatica* Salisb. (YJ, batch number: 20230807), *Artemisia caruifolia* Buch.-Ham. ex Roxb. (QH, batch number: 20231105), and *Prunella vulgaris* L. (XKC, batch number: 20231207)—from Beijing Tongrentang Co., Ltd. (Beijing, China). Verification of plant names was conducted through http://www.theplantlist.org and authenticated by Professor Zhenyue Wang (Heilongjiang University of Chinese Medicine, Harbin, China). All voucher specimens were deposited in the Herbarium of Heilongjiang University of Chinese Medicine.

The selected herbs were weighed appropriately for decoction preparation. TNX, JH, XB, and YJ were decocted with water at ratios of 10∶1 and 8∶1 for two cycles of two hours each. QH and XKC were decocted similarly, using water ratios of 10∶1 and 8∶1 for durations of one hour and one and a half hours, respectively. Subsequently, the decoctions were combined, concentrated, and dried under vacuum to yield the TNX/JH/XB/YJ/QH/XKC extracts, which were stored in the Chinese Medicine Chemistry Specimen Room of Heilongjiang University of Chinese Medicine (voucher specimen number: 20230830).

2.4. Animals

The Wistar rats (body weight = 200 ± 20 g, male) utilized in this study were procured from Beijing Vital River Laboratory Animal Technology Co., Ltd. (Beijing, China), under license No. SCXK(Beijing)2016-0006. The animals were kept in a controlled environment with unrestricted access to food and water, standard ventilation, a temperature maintained at 20 ± 3 °C, and relative humidity set at 55% ± 5%. A 12-hour light/dark cycle was implemented. All animal procedures were conducted in accordance with the ethical guidelines for animal experiments in China and received approval from the Ethics Committee for Experimental Animals at Heilongjiang University of Chinese Medicine, with the approval number 2023051903.

Following a week of acclimatization, the rats were randomly assigned to nine groups: a blank control group (K, n = 8), an AD model group (M, n = 8), a positive drug group (Y, n = 8), and three treatment groups corresponding to the warm TCMs (TNX, n = 8; JH, n = 8; XB, n = 8), as well as three control groups corresponding to the cold TCMs (YJ, n = 8; QH, n = 8; XKC, n = 8). Except for the blank control group, all rats were induced with AD through intraperitoneal injection of D-galactose (D-gal, 60 $mg{\cdot}kg^{-1}{\cdot}d^{-1}$) and oral administration of aluminum chloride ($AlCl_3$, 200 $mg{\cdot}kg^{-1}{\cdot}d^{-1}$) for 70 consecutive days [11]. The positive drug group received donepezil (3 $mg{\cdot}kg^{-1}{\cdot}d^{-1}$) orally. Treatment and control groups were administered the corresponding herbal extracts (TNX at 4.7 $g{\cdot}kg^{-1}{\cdot}d^{-1}$, JH at 2.8 $g{\cdot}kg^{-1}{\cdot}d^{-1}$, XB at 4.7 $g{\cdot}kg^{-1}{\cdot}d^{-1}$, YJ at 4.7 $g{\cdot}kg^{-1}{\cdot}d^{-1}$, QH at 5.6 $g{\cdot}kg^{-1}{\cdot}d^{-1}$, XKC at 7 $g{\cdot}kg^{-1}{\cdot}d^{-1}$) for a duration of 35 days. Dosages for each herb were derived from the adult oral dosages specified in the Chinese Pharmacopoeia and converted to rat equivalents using the standard body surface area method. Variations in dosages among the six herbs were based on their official dose ranges, medicinal potency, toxicity, and inherent properties. All administered doses fell within a safe and effective range to prevent toxic interference and ensure experimental comparability.

2.5. Behavioral tests

The spatial learning and memory capabilities of the rats were assessed using the Novel Object Recognition Test (NORT) [12] and the Morris Water Maze (MWM) [13] protocols. On day 62 of the drug administration timeline, a two-day NORT was performed. Commencing on day 64, the MWM assessment was conducted over six days, with the first five days devoted to training and the final day dedicated to a memory test. During the MWM test, the frequency with which the rats engaged with, traversed, or entered the escape platform area within a 60-second interval was recorded.

2.6. Sample collection and preparation

Following the completion of the behavioral tests, rats were weighed and anesthetized, after which blood was collected *via* the abdominal aorta. The samples were allowed to stand at room temperature for 2 h before being centrifuged at 3500 r·min^{-1} for 10 min. The supernatant was aliquoted and stored at −80 °C for subsequent analyses. After blood collection, euthanasia was conducted *via* cervical dislocation. The brains were quickly removed under sterile conditions, weighed, and the whole brains of three rats from each group were fixed in 4% paraformaldehyde solution for pathological examination. Remaining brain tissues were separated, and both the cortex and hippocampus were isolated in an ice bath and preserved at −80 °C. A portion of the hippocampal tissue was immersed in a 2.5% glutaraldehyde solution for transmission electron microscopy (TEM) analysis. Fresh fecal samples (1−2 pieces) from the colon were collected and frozen at −80 °C for DNA extraction to analyze gut microbiota.

2.7. Biochemical and pathological analyses

For histological examination, brain tissue fixed in 4% paraformaldehyde was processed into paraffin sections and subjected to hematoxylin and eosin (H&E) and Nissl staining to evaluate neuron morphology in the hippocampus and cortex. A 1 mm^3 block of fresh hippocampal tissue was fixed in glutaraldehyde at room temperature in the dark for 2 h and subsequently stored at 4 °C for transport. TEM was utilized to assess mitochondrial morphology, nuclear structure in the hippocampus, integrity of the myelin sheath, and architecture of synaptic complexes. Enzyme-linked immunosorbent assay (ELISA) kits were employed to quantify the levels of AChE, choline acetyltransferase (ChAT), superoxide dismutase (SOD), catalase (CAT), malondialdehyde (MDA), and glutathione peroxidase (GSH-Px) in hippocampal tissue.

Western blot analyses were conducted to determine the expression levels of brain-derived neurotrophic factor (BDNF) (ABclonal, A21176), sirtuin 1 (SIRT1) (Proteintech, 13161-1-AP), postsynaptic density protein 95 (PSD95) (Proteintech, 20665-1-AP), myelin-associated glycoprotein (MAG) (Proteintech, 14386-1-AP), AMP-activated protein kinase (AMPK) (ABclonal, AP1441), phosphorylated AMPK (p-AMPK) (ABclonal, A12718), β-actin (ABclonal, AC026), and glyceraldehyde-3-phosphate dehydrogenase (GAPDH) (Proteintech, 10494-1-AP in hippocampal tissue.

2.8. Untargeted plasma and brain metabolomic analysis

Non-targeted metabolomics analysis of rat plasma and hippocampal tissue was conducted utilizing the ACQUITY UPLC system (Waters, Milford, USA) in conjunction with the Q-TOF Synapt G2-SI mass spectrometer (Waters, Milford, USA). Detailed information on detection methods is available in the supplementary materials (Supplementary File 1: Methods).

2.9. 16S rRNA gene sequencing and analysis

Sterile fecal samples were collected for DNA extraction, followed by 2% agarose gel electrophoresis. PCR was performed using Phusion® High-Fidelity PCR Master Mix with GC Buffer and a high-fidelity enzyme. The PCR products were purified using magnetic beads, quantified through enzyme labeling, and then processed with the TruSeq® DNA PCR-Free Sample Preparation Kit for sequencing library construction. The library was sequenced on the NovaSeq6000 platform. Raw sequencing reads underwent filtering using Fastp (v0.22.0, https://github.com/OpenGene/fastp), and chimeric sequences were removed *via* FLASH (v1.2.11, http://ccb.jhu.edu/software/FLASH), resulting in a final valid dataset. Filtered data were then subjected to various classification analyses, including OTU clustering, ASV denoising, and species annotation. Additional analyses encompassed sample complexity evaluation, multi-sample comparisons, and functional annotation.

2.10. Quantitative proteomics analysis

Hippocampal tissue from rats was collected and promptly stored in liquid nitrogen. Proteins were extracted for quantitative proteomic analysis, with detailed methodologies provided in the supplementary materials (Supplementary File 1: Methods).

2.11. Analysis of the chemical composition of warm herbs

The identification of chemical components in warm-natured herbs was conducted using Q-Orbitrap high-resolution liquid chromatography-mass spectrometry. In brief, 100 μL of the extract was combined with 300 μL of methanol and vortexed for 10 min. The mixture was then centrifuged at 13 000 r·min^{-1} for 10 min, and the supernatant was collected for instrumental analysis. Compound names, molecular formulas, structural formulas, and peak areas were analyzed using the Compound Discover 3.3, mzCloud, and Progenesis QI databases. Specific chromatographic conditions and chemical identification methods are detailed in the supplementary materials (Supplementary File 1: Methods).

2.12. Statistical analysis

Statistical analysis was conducted using one-way and two-way analysis of variance (ANOVA), with statistical significance established at $P < 0.05$. All analyses were performed using GraphPad Prism 9.5.1 software.

3. Results

3.1. Data mining and Network pharmacological analysis results

A total of 88 articles were ultimately selected, encompassing 94 prescriptions and 141 herbs. The findings indicate that warm-natured herbs constituted a significant proportion of the potential herbal candidates. As illustrated in Fig. 1A, the core herbal combination for AD treatment identified comprises Acorus gramineus, *Polygala tenuifolia* Willd., and *Ligusticum sinense* ('Chuanxiong'), with all core drugs classified as warm/hot in nature.The herbs utilized for the treatment of AD primarily exhibit bitter, pungent, and sweet flavor profiles, and are mainly associated with the liver, kidney, and heart meridians (Fig. 1B).

After the removal of duplicates, a total of 25 bioactive compounds were identified within THPH (Fig. 2A), leading to the prediction of 545 unique targets. In TCPH, 47 bioactive compounds were identified (Fig. 2G), resulting in 644 potential targets for further analysis. A comprehensive collection of 1226 targets re-

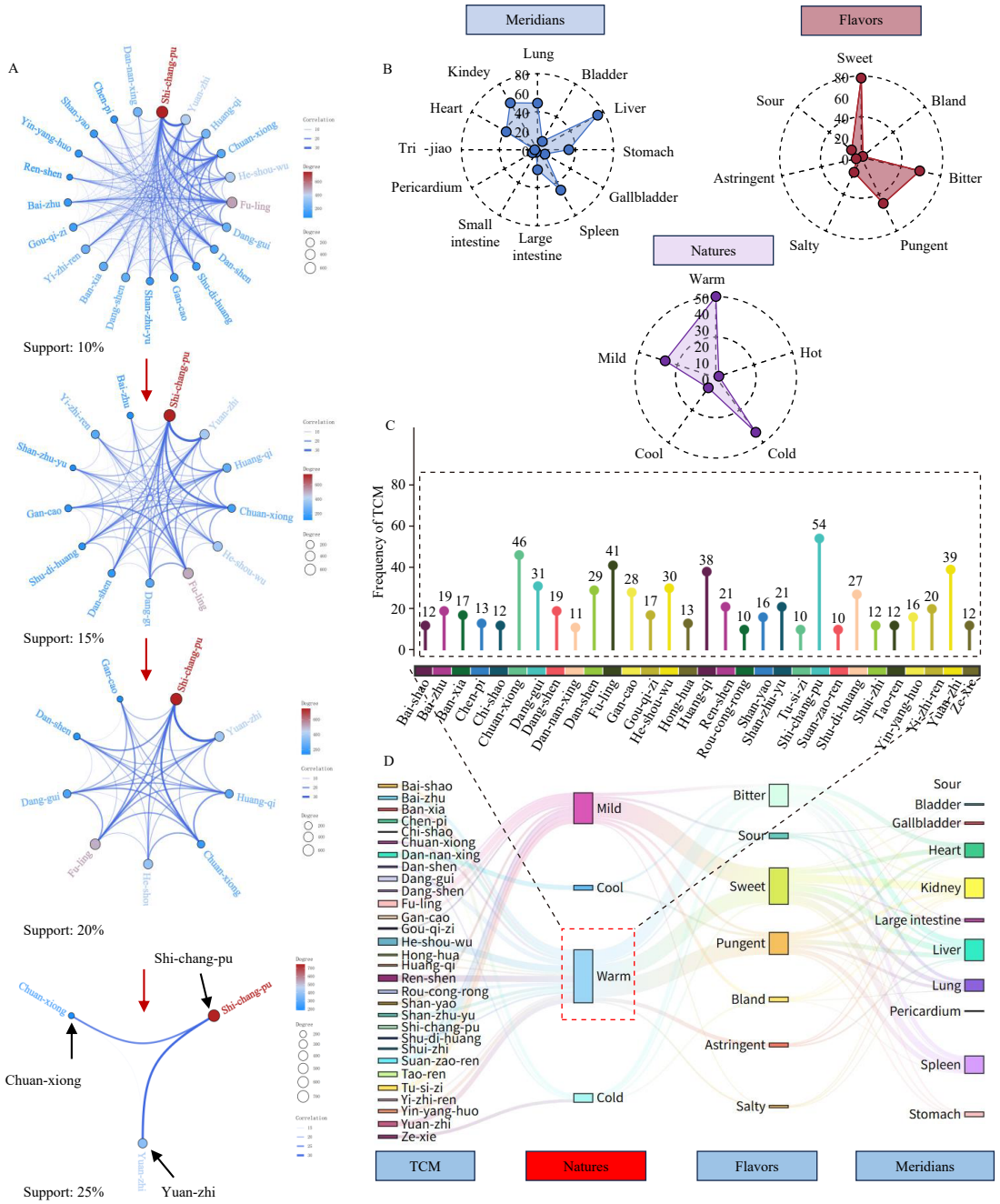


Fig. 1 Statistical results of the prescription analysis. (A) Network topology diagram of common drugs. (B) Properties and meridian tropism of herbs. (C) High-frequency herbs used to treat AD. (D) Relationships Among Properties (natures, flavors, meridians) of TCM.

lated to AD was obtained from disease-associated databases. Venn diagram analysis (Figs. 2B and 2H) identified 188 and 220 common targets among THPH, TCPH, and AD. These overlapping targets were utilized to construct a PPI network, comprising 214 nodes and 692 edges for THPH, and 268 nodes and 1325 edges for TCPH, thereby illustrating the interaction relationships among these targets (Figs. 2C and 2I). Key targets were determined based on their node degree values and included TP53, STAT3, AKT1, SIRT1, SRC, BDNF, HSP90AA1, EGFR, TNF, PIK3R1, and IL6. A separate PPI network for these key targets was constructed to visualize their interactions (Figs. 2D and 2J). KEGG pathway enrichment analysis of the common targets from THPH and TCPH highlighted significant associations with AD and various metabolic and signaling pathways, including lipid metabolism, energy metabolism, synaptic function, and inflammatory responses, such as the calcium signaling pathway, AMPK signaling pathway, mTOR signaling pathway, arachidonic acid metabolism, cholinergic synapse, long-term potentiation, long-term depression, sphingolipid signaling pathway, Toll-like receptor signaling pathway, efferocytosis, autophagy, and the HIF-1 signaling pathway (Figs. 2F and 2L). GO enrichment analysis further identified key biological processes, including responses to xenobiotic stimuli, regulation of inflammatory responses, cognition, regulation of synaptic plasticity, regulation of lipid metabolic processes, and regulation of apoptotic signaling pathways (Figs. 2E and 2K).

3.2. Effects of THPH and TCPH on memory loss in vivo

The short-term learning, spatial learning, memory capacity, and therapeutic effects of THPH and TCPH on AD rats were evaluated using NORT and MWM (Fig. 3A). As illustrated in Figs. 3H–3J, the NORT results indicated a significant reduction in the preference for novel objects (24 h) in the model group ($P < 0.05$

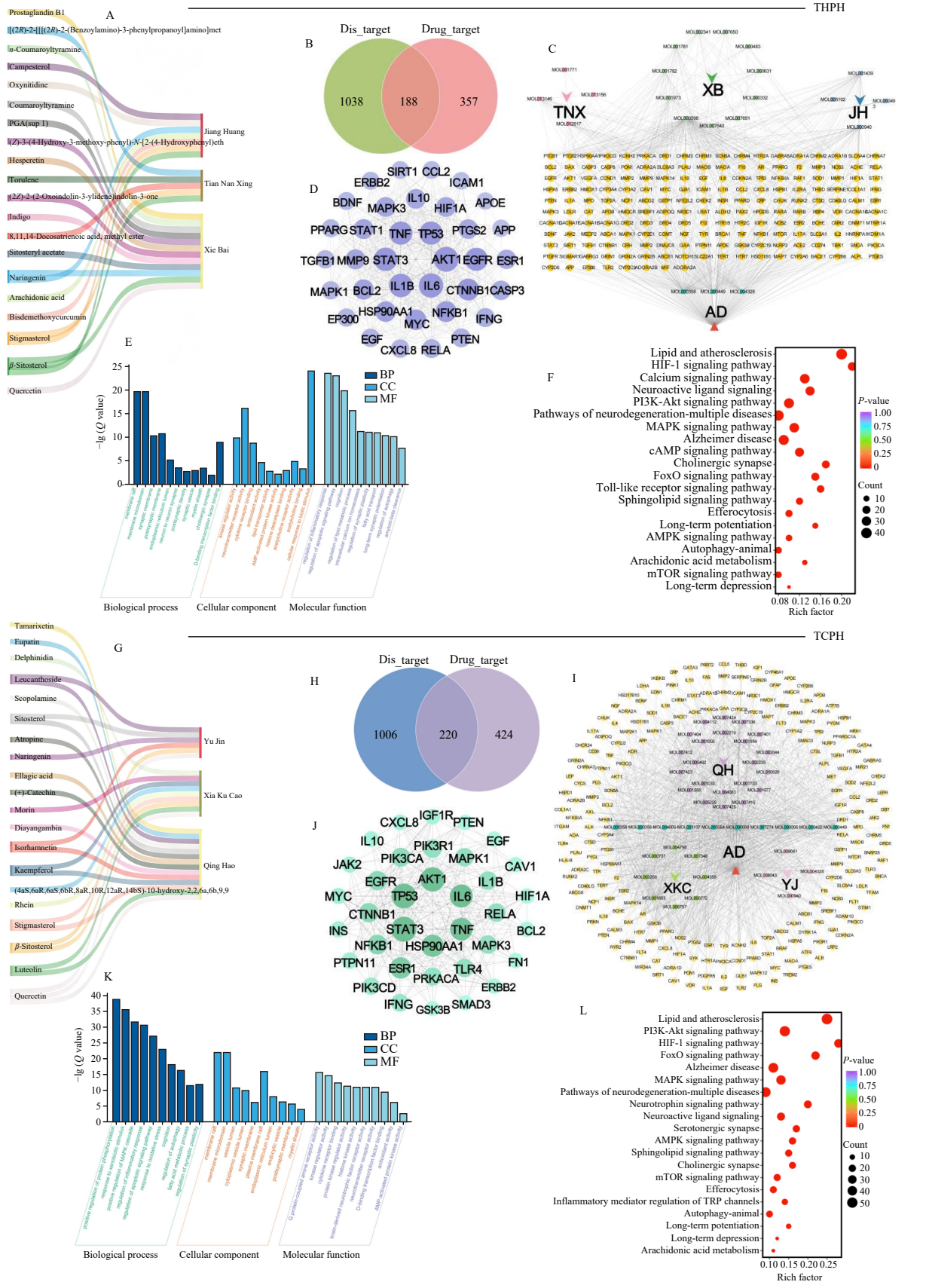


Fig. 2 Network pharmacological analysis of THPH, TCPH to improve AD. (A) Active ingredients of THPH and TCPH. (B, H) Venn diagram of common targets of THPH, TCPH and AD. (D, J) PPI network of potential target genes. (C, I) Target interaction network related to THPH, TCPH against AD. (E, F, K, L) KEGG pathway and GO function enrichment of overlapping targets.

and $P < 0.01$), demonstrating impaired learning and memory capabilities, thereby confirming successful model establishment. Treatment with THPH significantly alleviated short-term memory deficits in the rats, while TCPH did not produce notable improvements.

During the MWM spatial learning task, the escape latency

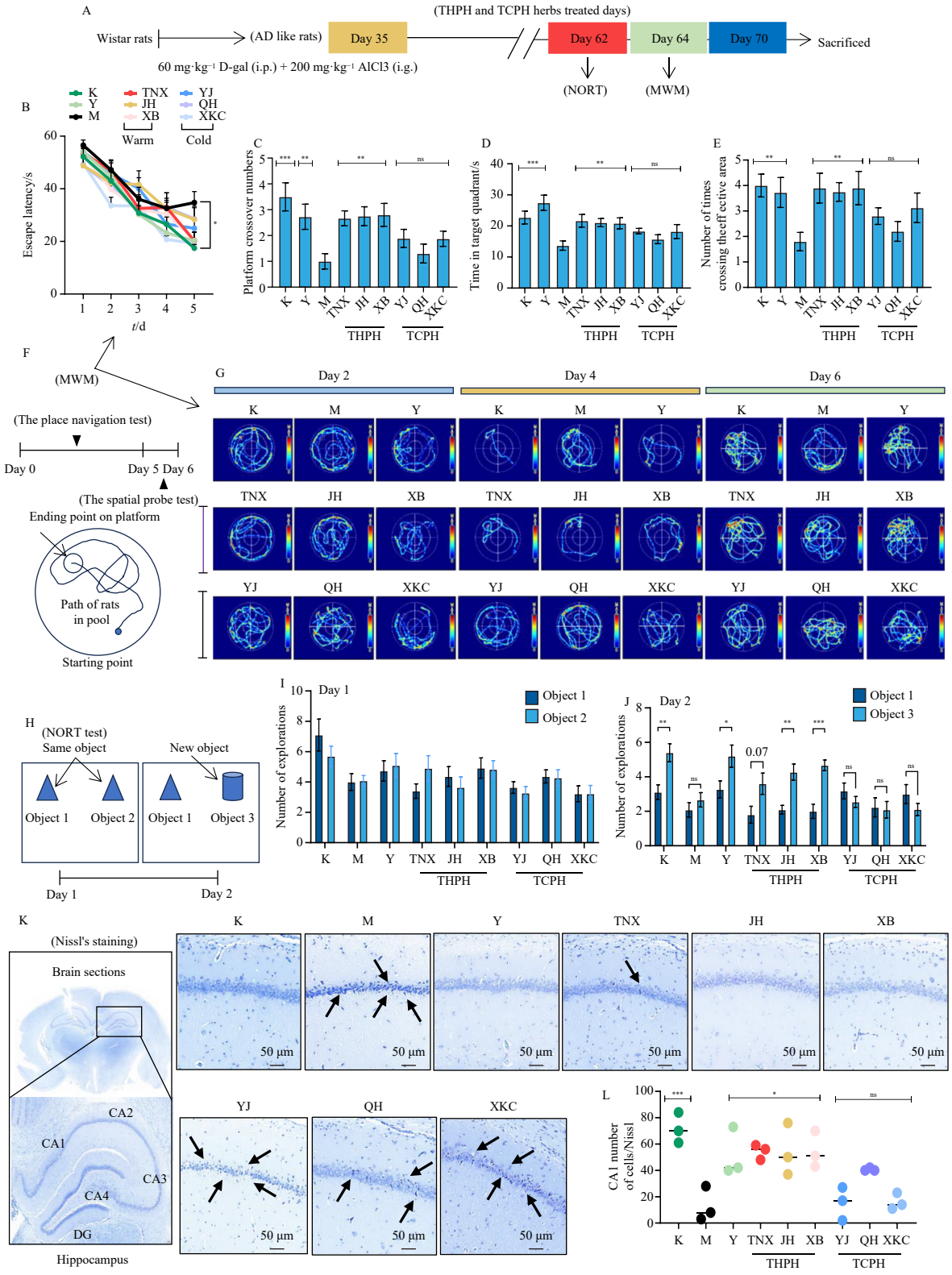


Fig. 3 Effects of THPH and TCPH on cognitive deficits in AD rats. (A) Timeline of experimental procedure. (B) The escape latency was counted and analyzed. (C) The frequency of platform crossings. (D) Time spent in the target quadrant. (E) The frequency of the effective area crossings. (F) Flowchart of the MWM Procedure. (G) The representative swimming trace of Place navigation test and probe test in MWM. (H) Flowchart of the NORT Procedure. (I–J) Quantitative results of the NORT. (K–L) Pathological section (Scale bar = 50 μm) and quantitative results of the hippocampus ($n = 3$). Black arrows denote injured neurons. The quantification of number of nissl bodies were normalized using number of number of Nissl bodies/CA1 area (mm^3). $^{*}P < 0.05$, $^{**}P < 0.01$, or $^{***}P < 0.001$ were considered significant.

progressively decreased across all groups as the training period progressed. As shown in Figs. 3B–3G, beginning on day 3 of the MWM test, rats in the model group displayed a significantly longer escape latency compared to the control group, characterized by aimless and confused swimming paths, further supporting the successful modeling. In the spatial exploration assessment, time spent in the target quadrant, the number of crossings in the effective area, and the number of platform crossings were significantly decreased in the model group compared to controls. THPH treatment markedly ameliorated these deficits, whereas TCPH did not demonstrate significant therapeutic effects.

3.3. The effect of THPH and TCPH on the morphology of neurons

HE and Nissl staining of the hippocampal CA1 regions revealed well-preserved hippocampal neurons in the blank control group, characterized by cellular alignment and intact cellular structures. In contrast, the neurons in the AD model group displayed damage, including a thinner CA1 pyramidal cell layer, a reduced number of neurons, and numerous cells exhibiting shrunken cytoplasm, condensed nuclei, and deep staining. Rats treated with THPH experienced significantly less neuronal loss, with cells appearing more compact and exhibiting fewer pathological alterations than those in the model group or TCPH (Figs. 3K and 4A).

As shown in Fig. 4E, TEM analysis further revealed severe degeneration of hippocampal nuclei in the AD model and TCPH groups, including nucleolar disruption, nuclear membrane distortion, and chromatin material degeneration. Conversely, the hippocampal nuclei in the blank control, positive drug, and THPH groups displayed intact or nearly normal nucleoli and nuclear membranes, with homogeneous chromatin distribution. These results suggest that THPH exerts a protective effect on hippocampal neurons and can reverse dementia-associated morphological changes in the hippocampus, while TCPH demonstrates limited therapeutic effects.

3.4. Effects of THPH and TCPH on cholinergic metabolism, oxidative damage, and mitochondrial morphology

Disturbances in the cholinergic system and oxidative stress are critical factors in the neuropathological progression of AD [14]. To evaluate these aspects, cholinergic factors (AchE and ChAT) and oxidative stress markers (GSH-Px, CAT, MDA, and SOD) were measured in the brain tissues of rats from the blank control, AD model, and treatment groups. As illustrated in Figs. 4B–4D, there was a significant increase in AchE activity and a decrease in ChAT levels in the brain tissues of AD rats, indicating cholinergic impairment. Conversely, treatment with THPH resulted in a significant increase in ChAT activity and a decrease in AchE activity compared to the AD group. In contrast, TCPH did not produce significant alterations in ChAT or AchE levels. Furthermore, exposure to D-galactose and $AlCl_3$ induced a marked oxidative stress response, as evidenced by significant reductions in CAT, GSH-Px, and SOD levels, along with a notable increase in MDA levels in the AD group. These oxidative disturbances were reversed following THPH administration (Figs. 4F–4I). Notably, while XB exhibited no significant effect on MDA levels, there was a tendency toward reduction. Among the TCPH treatments, QH increased GSH-Px activity, while YJ enhanced SOD levels, although these effects were less pronounced compared to those observed with THPH.

Mitochondria, which are central to bioenergetics and oxidative stress, play a pivotal role in cellular function and survival [15]. As shown in Fig. 4J, TEM analysis revealed that healthy mitochondria typically displayed an ovoid or round shape, with a dense and homogeneous matrix, intact double membranes, and well-structured cristae. In contrast, mitochondria in AD rats exhibited significant damage, including ruptured double membranes, disrupted cristae, and mitochondrial collapse, indicating severe mitochondrial dysfunction. Treatment with THPH mitigated these mitochondrial abnormalities. However, in rats treated with TCPH, mitochondrial damage remained evident, characterized by abnormal vacuolated mitochondria (YJ group), rupture of the double membrane (QH group), degenerated mitochondria (XKC group), and disruption of cristae (observed in the YJ, QH, and XKC groups). These results suggest that THPH exerts a more pronounced effect on modulating cholinergic dysfunction, maintaining oxidative balance, and protecting mitochondrial integrity and function in AD model rats when compared to TCPH.

3.5. Effects of THPH and TCPH on myelin and synaptic plasticity damage

Synaptic plasticity impairments and demyelination represent early pathological features of AD [16]. TEM analysis was conducted to examine the ultrastructure of the myelin sheath (Fig. 5B). The hippocampus of the blank control group displayed intact and densely packed myelin sheaths. In contrast, the AD model group exhibited significant myelin degeneration, disintegration, and dispersion of the dense layer, along with thinning of the lamellar structure and axonal atrophy. Following THPH administration, a noticeable reduction in myelin loss was observed, with axonal atrophy exhibiting relatively less severity. However, treatment with TCPH did not yield significant improvements in these morphological changes. These findings suggest that THPH promotes myelin repair and has the potential to alleviate axonal damage.

Further analysis of hippocampal synapse ultrastructure (Fig. 5A) revealed that blank control rats had a higher number of well-defined, structurally intact synapses. In contrast, AD rats demonstrated a marked decrease in synapse quantity, with many connections appearing irregular and synaptic outlines blurred due to the dissolution of synaptic structures. THPH treatment resulted in significant restoration of synaptic integrity, evidenced by an increased number of synapses and mitochondria.

3.6. THPH improved dysregulation of brain and serum metabolites in AD rats

Peripheral and central metabolic disturbances are critical aspects of AD pathophysiology [17]. Principal component analysis (PCA) score plots indicated a clear separation between THPH and both the normal and model groups (Fig. 5C). THPH was closest to the K group, suggesting that D-galactose and $AlCl_3$ disrupted the brain and serum metabolic profiles of rats, and that THPH treatment improved these disturbances. Based on the combined results from behavioral tests, biochemical indices in brain tissues, histopathological examinations, and Metabolic profile, THPH exhibited a significantly greater therapeutic effect on AD symptoms compared to TCPH. Hence, THPH was selected for further investigation.

Additionally, orthogonal partial least squares discriminant analysis (OPLS-DA) was employed to identify differential metabolites related to pathological features and working mechanisms, following predefined criteria ($VIP > 1$; $P < 0.05$). The OPLS-DA score plots revealed significant differences between the K group and each individual THPH treatment compared to the M model (Supplementary File 3: Figures). This study identified a total of 21 specific brain metabolic biomarkers and 24 specific serum metabolic biomarkers (Figs. 5D–5E) associated with both AD models and THPH treatment, including Arachidonic Acid, Leukotriene A4, Phytosphingosine, Isocitric acid, LysoPC(16:0), sn-glycero-3-Phosphoethanolamine, Glutathione, Linoleic acid, Raffinose, myo-Inositol, Thiamine, Bilirubin, Cholic acid, etc. Metabolic function and pathway alterations in AD rats, as well as those treated with the warm herbs, were further analyzed using the KEGG database and Metabo-Analyst. A total of 21 pathways were enriched in brain metabolomics (Fig. 5F) and 24 pathways in serum metabolomics (Fig. 5G). Among these, THPH significantly regulated five metabolic pathways, including arachidonic acid metabolism, sphingolipid metabolism, the tricarboxylic acid (TCA) cycle, steroid hormone metabolism, and retinol metabolism (Fig. 5H).

3.7. THPH regulated gut microbiota dysbiosis in AD rats

To investigate the composition of the gut microbiota in AD rats and the effects of herbal treatments with warm properties, 16S rDNA sequencing was performed on fecal samples from

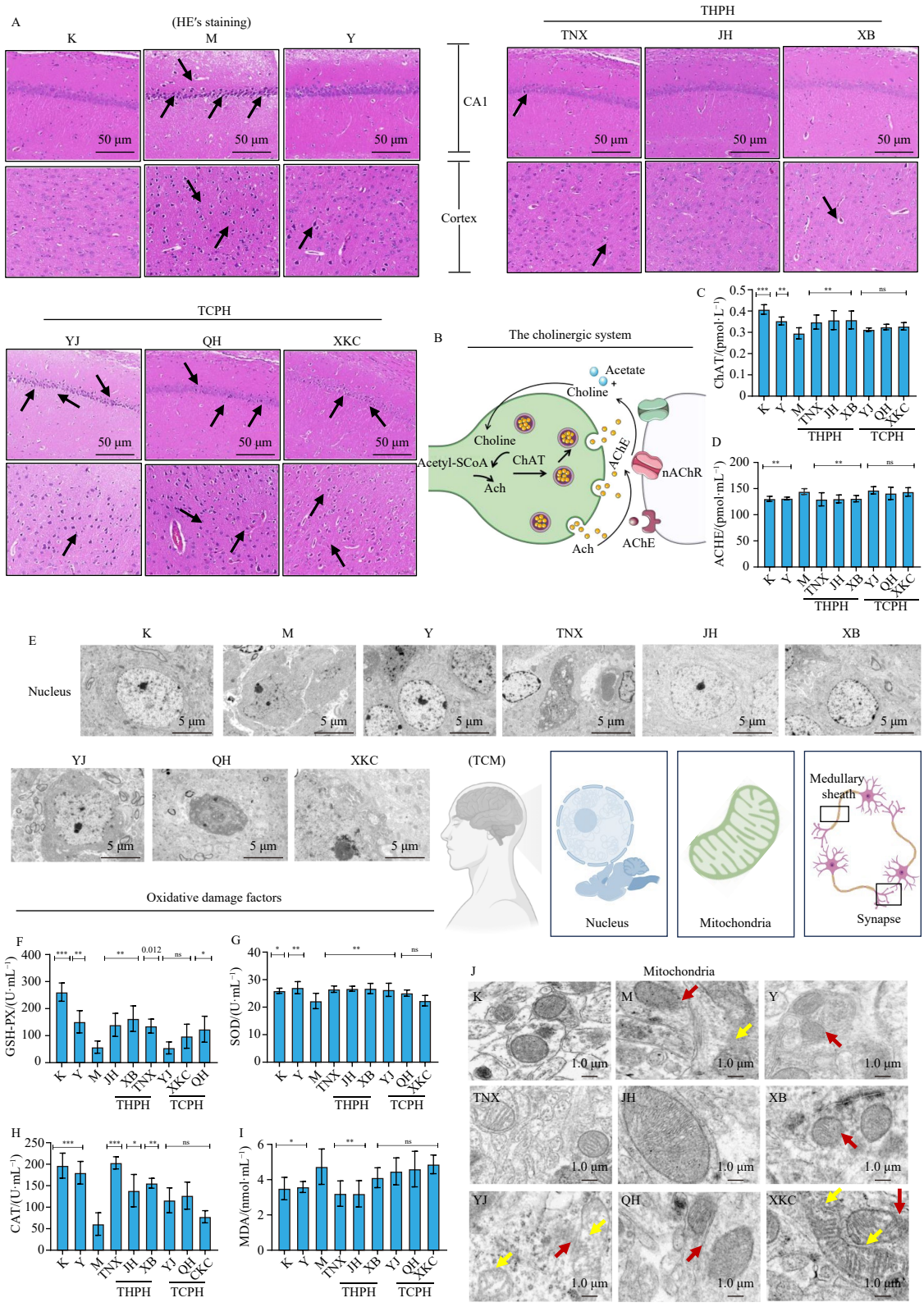


Fig. 4 Effects of THPH and TCPH on the cholinergic system, oxidative stress and neuron damage. (A) Representative HE staining images (Scale bar = 50 μm). (B) Physiology of the cholinergic synapse. (C–D) ELISA assay the levels of AchE and ChAT. (E) A representative images of nucleus abnormalities. (F–I) The levels of GSH-PX, SOD, CAT and MDA in each group. (J) The electron micrographs of Mitochondria. Data were represented as mean ± SD, $n = 7$. $^{*}P < 0.05$, $^{**}P < 0.01$, or $^{***}P < 0.001$ were considered significant. (Black arrows denote injured neurons; Red arrow: rupture of mitochondrial double membrane; Yellow arrow: destruction of cristae).

groups K, M, Y, and those treated with the warm herbs TNX, JH, and XB. α-Diversity (Figs. 6A–6D) index analysis indicated that the Simpson, ACE, Shannon, and Chao1 indices were significantly lower in the M group compared to the K group, reflecting reduced richness and diversity of the gut microbiota in the AD model. Following THPH intervention, the ACE, Shannon, Simpson, and Chao1 indices were significantly elevated, suggesting a positive effect of THPH on gut microbiota homogeneity and diversity. Additionally, β-diversity analysis (Fig. 6E), incorporating NMDS and PCoA, demonstrated significant divergence of the M group from the K group, while the THPH group was separated from the M group and clustered closer to the blank control group. After elim-

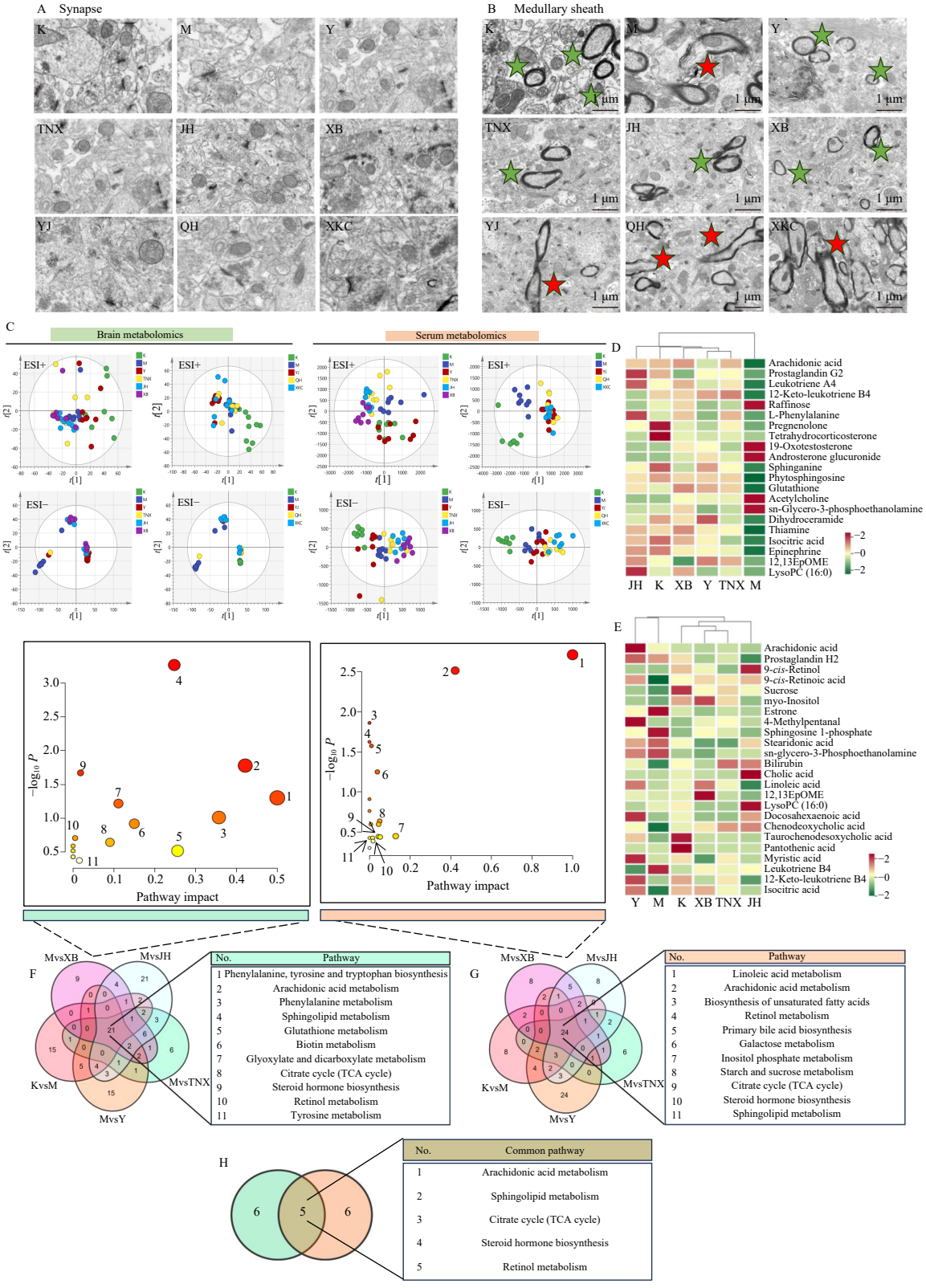


Fig. 5 Effects of THPH and TCPH on myelin damage, synaptic plasticity and metabolic profile. (A–B) The electron micrographs of Synapses, Myelin sheath. (C) PCA score plots. Heatmaps of different metabolites in brain metabolomics (D) and serum metabolomics (E). Metabolism pathway analysis in brain metabolomics (F) and serum metabolomics (G). (H) The common metabolic pathways of brain metabolomics and serum metabolomics.

inating background noise, the characteristic intestinal flora composition for each group was determined, revealing a total of 942 operational taxonomic units (OTUs) across the six groups (K: 1965; M: 1925; Y: 1393; TNX: 995; JH: 812; XB: 872), as shown in Fig. 6F. This indicates that dysbiosis induced by D-galactose and AlCl3 was partially restored by THPH.

To further elucidate the impact of THPH on the gut microbiome of AD rats, analyses of bacterial phylum classes, orders, families, and genus structures were conducted. At the phylum level, the predominant microorganisms in groups K, M, Y, TNX, JH, and XB were identified as Firmicutes, Bacteroidota, Proteobacteria, Desulfobacterota, and Verrucomicrobiota (Fig. 6H), with Firmi-

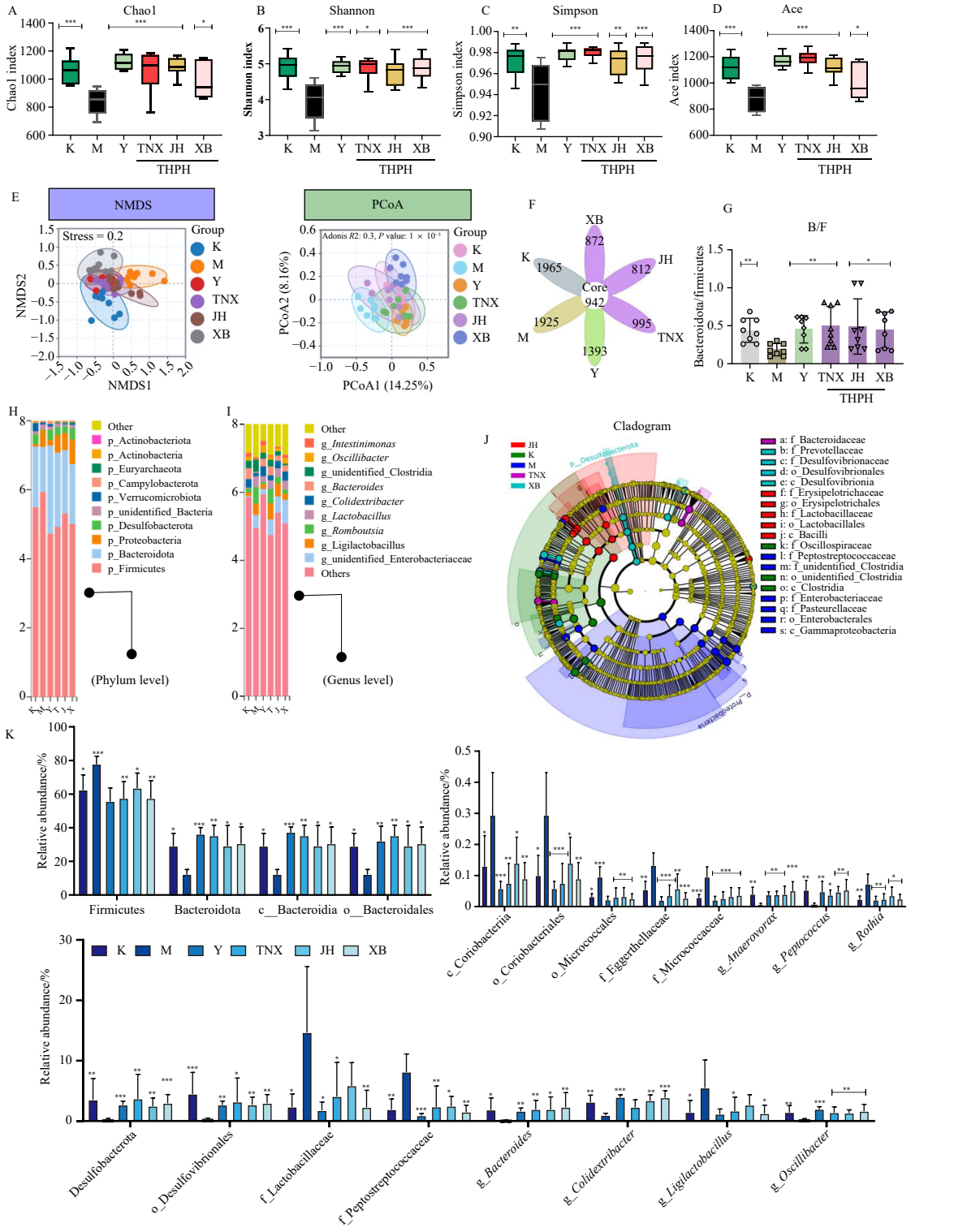


Fig. 6 Effect of THPH on intestinal flora. Alpha diversity estimators calculated indexes of Chao (A), Shannon (B), Simpson (C) and Ace (D) on OTUs level. (E) The PCoA among K, M and warm TCMs groups based on Weighted-Unifrac; The NMDS among the K, M and warm TCMs groups based on Bray Curtis. (F) Venn diagram of the common or the unique ASVs/OTUs. (G) The ratio of Firmicutes/Bacteroidetes. (H) Histogram of phylum abundance among groups. (I) Histogram of genus abundance among groups. (J) LEfSe analysis of relative abundance of gut microbiome. (K) Relative abundances of gut microbiota at the Phylum, Class, Order, Family and Genus levels, respectively. Data were represented as mean ± SD, $n = 7$. $^{*}P < 0.05$, $^{**}P < 0.01$, or $^{***}P < 0.001$ *vs* model group.

cutes, Bacteroidota, and Proteobacteria being the most dominant. A reduced Bacteroidota/Firmicutes (B/F) ratio is widely recognized as indicative of gut dysbiosis. As illustrated in Fig. 6G, the B/F ratio decreased in AD rats, while THPH administration resulted in an increased B/F ratio. In AD rats, Firmicutes levels were elevated, whereas Desulfobacterota and Bacteroidota were significantly reduced. Treatment with THPH effectively restored gut microbiota diversity by decreasing the abundance of Firmicutes and increasing the levels of Desulfobacterota and Bacteroidota, suggesting that THPH may alleviate cognitive and memory deficits through the modulation of these bacterial taxa.

At the genus level, further analysis revealed changes in the relative abundance of specific species. The stacked bar graph (Fig. 6I) shows that D-gal and $AlCl_3$-induced AD rats exhibited an increase in the abundance of *Rothia*, *Romboutsia*, and *Ligilactobacillus*, while *Oscillibacter*, *Peptococcus*, *Colidextribacter*, *Acetati-*

factor, *Bacteroides*, and *Anaerovorax* were significantly reduced. Administration of THPH reversed these changes, as depicted in Fig. 6K. These results suggest that THPH can modulate D-gal- and $AlCl_3$-induced alterations at multiple taxonomic levels, improving gut microbial dysbiosis and potentially contributing to therapeutic effects in AD rats.

3.8. THPH altered the proteomics profile of AD rats

The qualitative and quantitative analysis of the protein indicated that the result quality met the standards (Figs. 7A–7D and 7F). PCA of the identified proteins showed a distinct separation between the AD group and the control group, with a degree of reversal in the protein expression pattern observed after THPH treatment (Fig. 7E). Differentially expressed proteins (DEPs) were identified using a threshold of fold change > 1.2 or < 0.83 with $P < 0.05$ (Figs. 7G–7K). This analysis revealed 88 upregulated and 88 downregulated proteins. A comparison between the AD and TNX groups identified a total of 124 proteins, with 62 upregulated and 62 downregulated. Between the AD and JH groups, 158 proteins were identified, including 92 that were upregulated and 66 downregulated. The comparison of the AD and XB groups yielded a total of 206 proteins, comprising 108 upregulated and 98 downregulated proteins. Overlaps of DEPs among the different groups indicated 20 common DEPs in the control, AD, and TNX groups; 25 common DEPs in the control, AD, and JH groups; and 32 common DEPs in the control, AD, and XB groups (Fig. 7L). The quantification of DEPs is depicted in Figs. 7M–7O. Hierarchical clustering analysis of these proteins revealed that THPH significantly reversed the expression trends of most proteins compared to the AD group, including Lpin1, Camk2d, Elovl2, SEL1L, Sorbs1, Ankrd50, IL1RAP, Klhdc7a, Grik3, Smad1, Nubp1, Heph, Stau1, Gda, Marcksl1, Ccn3, Elac1, Fibp, Kif1c, Crhbp, Pggt1b.

GO enrichment analysis indicated that the proteins influenced by THPH were primarily located in synapses (axons and dendrites) and were significantly involved in neuronal protection (Fig. 8A and Supplementary File 3: Figures). KEGG analysis further highlighted that the signaling pathways related to the differential proteins between the model and THPH groups were predominantly associated with autophagy, energy metabolism-related pathways (AMPK), Efferocytosis, Calcium signaling pathway, mTOR signaling pathway, Glycerophospholipid metabolism, Glycerolipid metabolism, IL-17 signaling pathway, HIF-1 signaling pathway, cAMP signaling pathway, and cholinergic synapses (Fig. 8A and Supplementary File 3: Figures).

3.9. Correlations between risk factors, metabolites, and microorganisms

To explore the potential relationships among risk factors, metabolites, proteins, and gut microbiota, Spearman's correlation analysis was conducted to examine interactions between fecal differential bacteria, risk factors, and differential metabolites (Supplementary File 3: Figures). The analysis revealed that brain metabolite-gut microbiota interactions were significantly influenced by THPH treatment. Eleven microbial taxa exhibited strong associations with specific differential metabolites, with positive correlations observed for sphinganine, dihydroceramide, isocitric acid, 12-keto-leukotriene B4, and glutathione (GSH). Conversely, negative correlations were identified with raffinose, 19-oxotestosterone, androsterone glucuronide, acetylcholine (ACh), and sn-glycero-3-phosphoethanolamine.

ChAT and antioxidant enzyme activities (CAT, GSH-Px, and SOD) displayed significant positive correlations with various brain metabolites, including arachidonic acid, prostaglandin G2, 12-keto-leukotriene B4, GSH, sphinganine, dihydroceramide, and isocitric acid. In contrast, significant negative correlations were observed with lysoPA (0:0/18:2 (9*Z*,12*Z*)), lysoPA (20:3 (5*Z*,8*Z*,11*Z*)/0:0), cortisol, and androsterone glucuronide. Moreover, activities of ChAT and antioxidant enzymes (CAT, GSH-Px, and SOD) correlated significantly with most intestinal microbiota, whereas AChE and MDA exhibited opposite correlations with these metabolites and gut flora. In conclusion, Spearman's correlation analysis suggests that THPH interventions improve cognitive deficits in AD by modulating metabolic and gut flora imbalances, thereby reducing cholinergic deficits and oxidative stress.

3.10. Effects of THPH on protein levels related to energy metabolism, oxidative stress, and synaptic plasticity

Western blot analysis indicated that induction with D-galactose and $AlCl_3$ significantly reduced the expression levels of p-AMPK, Nrf2, the myelin-associated protein MAG, the synaptic protein SIRT1, BDNF, and PSD95 in the hippocampus of AD model rats, while AMPK protein levels remained unchanged. SIRT1, PSD95, and BDNF have been recognized as key factors in synaptic plasticity and memory formation [18]. Following intervention with THPH, the expression levels of p-AMPK, Nrf2, MAG, SIRT1, BDNF, and PSD95 were significantly increased ($P < 0.05$, $P < 0.01$, $P < 0.001$), as depicted in Figs. 8B–8C. These results suggest that THPH can alleviate myelin loss and synaptic damage in AD to varying extents, improving energy metabolism and mitigating oxidative stress through the AMPK/Nrf2 signaling pathway.

3.11. Chemical composition of THPH

Additionally, component analysis identified 103 components in TNX, 81 components in JH, and 89 components in XB (Supplementary File 2: Tables). The characteristic profiles of total ion chromatography and decomposition pathways for TNX, JH, and XB, in both positive and negative signal modes, are presented in the supplementary materials (Supplementary File 3: Figures).

4. Discussion

Currently, limited literature has systematically applied statistical methods to analyze the application patterns of TCM in the treatment of AD. In light of this gap, core herbal properties and drugs were identified through data mining technology. Our research findings indicate that warm-natured herbs are the most commonly utilized. Among these, three core medicines identified (*Acorus gramineus*, *Polygala tenuifolia* Willd., and *Ligusticum sinense* 'Chuanxiong') are warm-natured herbs. Network pharmacology analysis predicted 545 and 644 potential targets for THPH and TCPH, respectively, with 188 and 220 overlapping with a set of 1226 AD-related targets. Enrichment analysis suggested that THPH and TCPH may exert their anti-AD effects primarily through modulation of lipid metabolism, energy metabolism, synaptic function, and inflammatory response signaling pathways, as well as other associated pathways. These findings support further investigation into the therapeutic mechanisms of warmth in AD model rats (Fig. 9).

Although the brain constitutes only 2% of total body mass, it consumes 20% of the body's oxygen and 25% of its glucose, reflecting its high energy demands for functions such as learning, memory, and motor control [19]. Mitochondria, as the central energy source of the CNS producing 95% of its energy [20], and cholinergic synapses, critical for synaptic plasticity and long-term memory [21], are key components. The majority of brain energy supports synaptic activity through mitochondrial ATP production. AMPK serves as a vital regulator of energy metabolism, enhancing mitochondrial function and reducing neuronal oxidative damage [22]. As aging progresses, brain energy metabolism de-

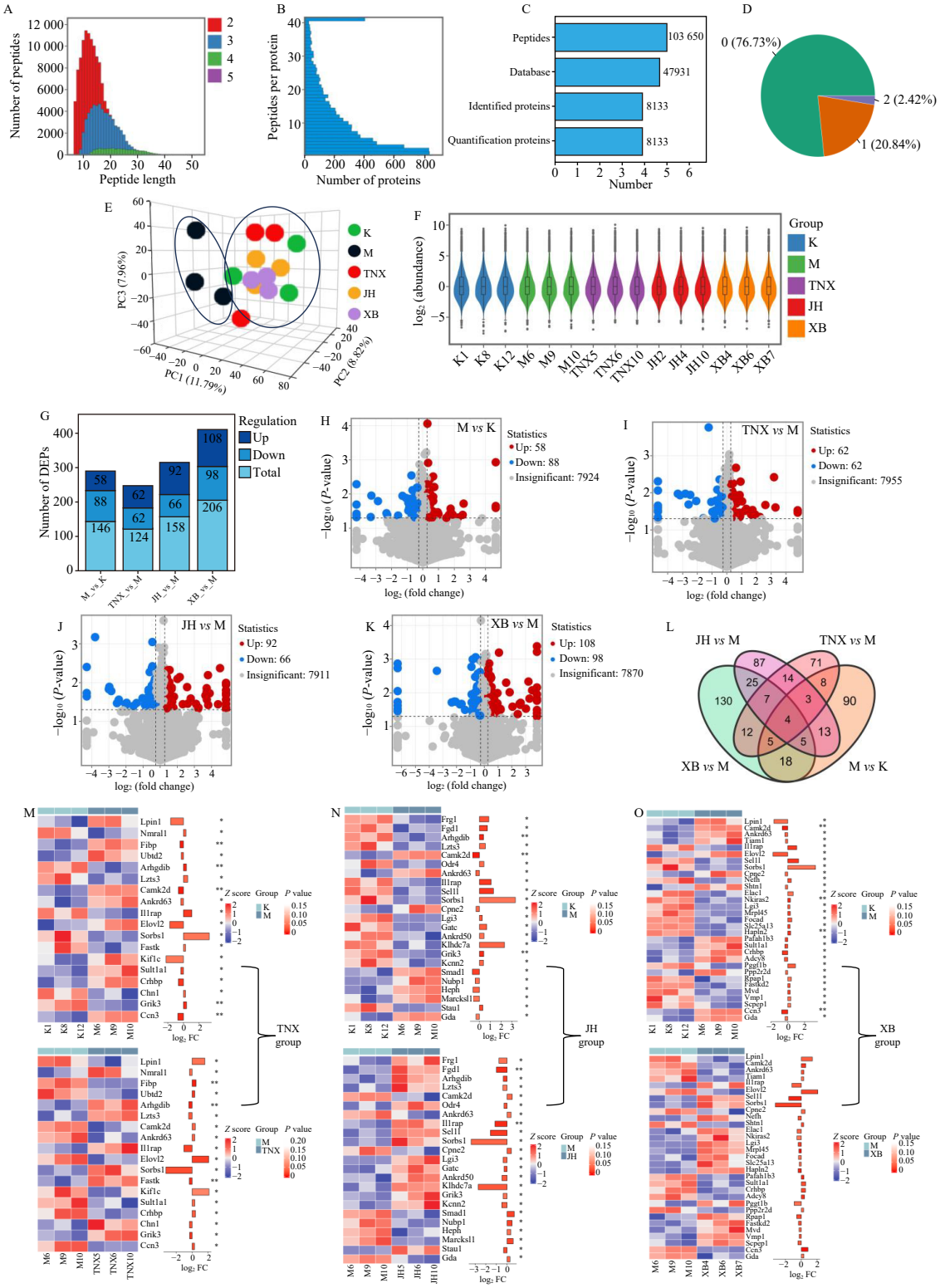


Fig. 7 Functional classification of proteomic data by bioinformatic analysis. (A–D) Quality assessment of protein qualitative results. (E) PCA of the K, M, warm TCMs groups. (F) Quality assessment of protein quantification results. (G) Number of DEPs in each group. (H–K) Volcano plot for the M group *vs* the K, TNX, JH and XB groups. (L) Venn diagram of the enriched DEPs. (M–O) Heatmap of DEPs content.

clines, resulting in reduced neuronal glucose uptake and mitochondrial dysfunction—particularly evident in AD [23]. This energy imbalance accelerates synaptic loss, cognitive impairment, and the pathological progression of AD [24]. Our research demonstrated that AD model rats exhibited impaired mitochondrial morphology, compromised hippocampal myelin sheaths, and altered synaptic structures, along with decreased levels of energy metabolism biomarkers (e.g., isocitric acid, L-phenylalanine, sphinganine, thiamine, myo-inositol, D-galactose, sucrose, and alpha-D-glucose). Although total AMPK levels remained unchanged, p-AMPK levels significantly decreased, confirming energy metabolism dysfunction in the pathogenesis of AD. Treatment of AD model rats with THPH resulted in improved integrity of mitochondria and myelin sheaths, increased synapse counts, normalization of energy metabolism biomarkers, activation of AMPK phosphorylation (thereby elevating p-AMPK), and upregulation of synapse-as-

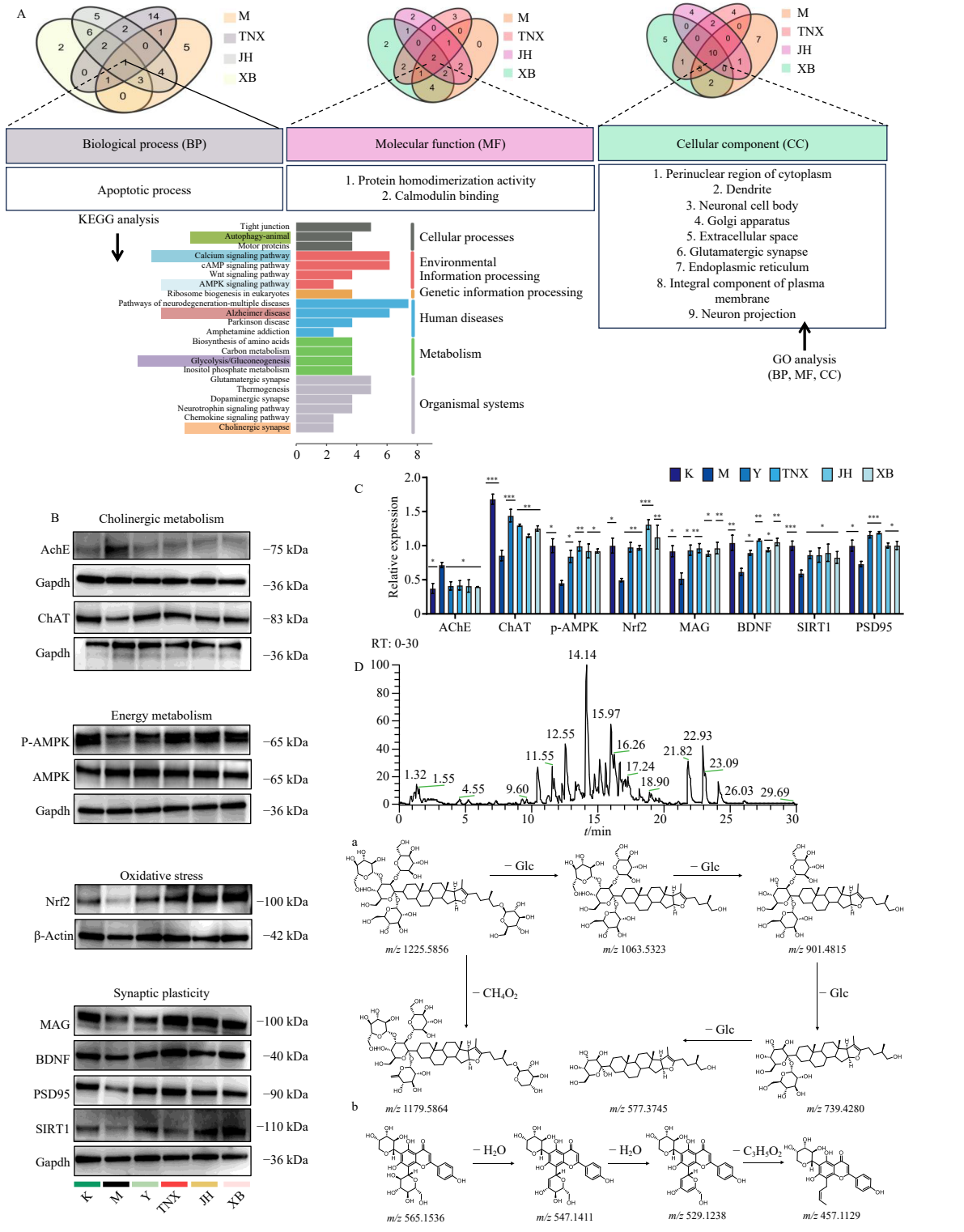


Fig. 8 Identification and analysis of the related proteins, pathways and chemical components regulated by THPH. (A) GO enrichment, KEGG pathway analysis of the DEPs. (B–C) Validation of the expression of ACHE, ChAT, BDNF, SIRT1, PSD95, MAG, Nrf2, AMPK, p-AMPK proteins in hippocampal tissue through Western blotting. (D) Chemical composition of THPH.

sociated proteins (including SIRT1, PSD-95, SYN, and BDNF). These findings suggest that THPH alleviates energy metabolism dysfunction related to AD and promotes synaptic plasticity.

Synapses serve as the primary sites of neuronal communication, facilitating the transfer of neurotransmitters from presynaptic axon terminals to postsynaptic neurons. Among the various neurotransmitters, ACh plays a critical role in memory; it is synthesized by ChAT and degraded by AChE [25]. Cholinergic dysfunction is considered a hallmark of AD. In AD, increased AChE activity accelerates the breakdown of ACh, impairing cholinergic transmission and contributing to cognitive deficits [26]. Consequently, inhibiting AChE, enhancing ChAT activity, and restoring synaptic function have emerged as key therapeutic strategies. Administration of THPH effectively increased ACh concentrations in the synaptic cleft by significantly reducing AChE activity and enhancing ChAT levels, thereby improving cholinergic neurotransmission. Moreover, impaired synaptic plasticity and function contribute to oxidative stress in the brain. This oxidative

stress results from an imbalance between antioxidants and pro-oxidants and can even precede amyloid beta (Aβ) pathology [27]. Key antioxidants, such as SOD, GSH, and CAT, scavenge free radicals and reflect the extent of lipid peroxidation. Excessive reactive oxygen species (ROS) induced by oxidative stress lead to mitochondrial damage, deplete GSH, elevate MDA levels, and accelerate lipid peroxidation, all while disrupting glucose transporters and impairing glucose utilization [28, 29]. In our study, AD rats exhibited significantly decreased levels of GSH, as well as reduced activities of GSH-Px, CAT, and SOD, along with increased MDA levels, indicating weakened antioxidant capacity. Additionally, ceramide accumulation amplified oxidative stress, decreasing levels of dihydroceramide, which was significantly reduced in AD rats [30]. Lowered antioxidant metabolites, including bilirubin [31] and isocitric acid [32], further indicated impaired antioxidant capacity. Abnormal metabolism of tyrosine [33], arachidonic acid [34], and linoleic acid [35] exacerbated inflammation and oxidative stress. Treatment with THPH restored levels of dihydroceramide, bilirubin, and isocitric acid, reversed metabolic disorders, lowered MDA levels, enhanced antioxidant enzyme activities, and restored redox balance, suggesting that THPH can effectively suppress oxidative stress induced by D-galactose and $AlCl_3$.

Conversely, treatment with TCPH failed to ameliorate cognitive impairment in AD model rats, exhibiting a counteractive therapeutic effect compared to THPH and even leading to more severe cognitive deficits (Fig. 2G). This lack of efficacy may be primarily attributed to the inability of TCPH to alleviate D-galactose and $AlCl_3$-induced damage to the hippocampal nuclei, neurons, and mitochondria. Furthermore, relative to the model group, the TCPH group displayed more pronounced axonal atrophy and damage within the myelin sheath (Fig. 5A), accompanied by no observable increase in the number of synapses (Fig. 5B). Additionally, TCPH did not significantly reverse the aberrant expression of cholinergic factors (AChE, ChAT) or oxidative stress markers (SOD, GSH, CAT, MDA), leading to persistent cholinergic dysfunction (the abnormal expression of AchE and ChAT leads to the disorder of Ach synthesis and release [36]) and unresolved oxidative damage in AD rats. Given that Alzheimer's disease is a multidimensional, pathologically heterogeneous disorder, these etiological factors may act synergistically, promoting and causally reinforcing one another to perpetuate a vicious cycle [37], thereby further exacerbating memory deficits and cognitive impairment.

The gut microbiota plays a pivotal role in maintaining brain energy homeostasis *via* the gut-brain axis. Disruptions in the gut microbiome can exacerbate synaptic damage and accelerate cognitive decline [38]. In healthy individuals, Firmicutes and Bacteroidota dominate the gut microbiome, supporting energy metabolism and nutrient absorption. However, this composition is significantly altered in AD [39]. A higher B/F ratio is beneficial for maintaining intestinal homeostasis and may slow AD progression. In AD rats, an increase in Firmicutes and a decrease in Bacteroidota resulted in a lowered B/F ratio; however, these dysbioses were significantly reversed by THPH treatment, restoring the B/F ratio. THPH treatment significantly increased the abundance of beneficial genera such as *Oscillibacter*, *Peptococcus*, *Colidextribacter*, *Acetatifactor*, *Bacteroides*, and *Anaerovorax*, while reducing levels of *Rothia*, Romboutsia, and *Ligilactobacillus*. *Romboutsia* and *Oscillibacter* are associated with inflammation, and regulating their abundance can help improve inflammatory responses [40, 41]. *Colidextribacter* promotes the production of short-chain fatty acids (SCFAs), which alleviate intestinal inflammatory injury [42]. Although the function of *Acetatifactor* remains unclear, it is known as a butyrate-producing bacterium [43]. Butyrate can cross the blood-brain barrier, imparting anti-inflammatory, antioxidant, and immune-enhancing effects in AD while regulating histone acetylation to inhibit inflammation. Therefore, the potential therapeutic role of *Acetatifactor*, as a beneficial gut microbe in AD, warrants further investigation. SCFAs help maintain the integrity of the intestinal barrier and mitigate AD pathology, and *Anaerovorax*, another SCFA-producing bacterium, contributes to these protective effects [44]. These findings support the conclusion that THPH can effectively regulate gut microbiota dysbiosis asso-

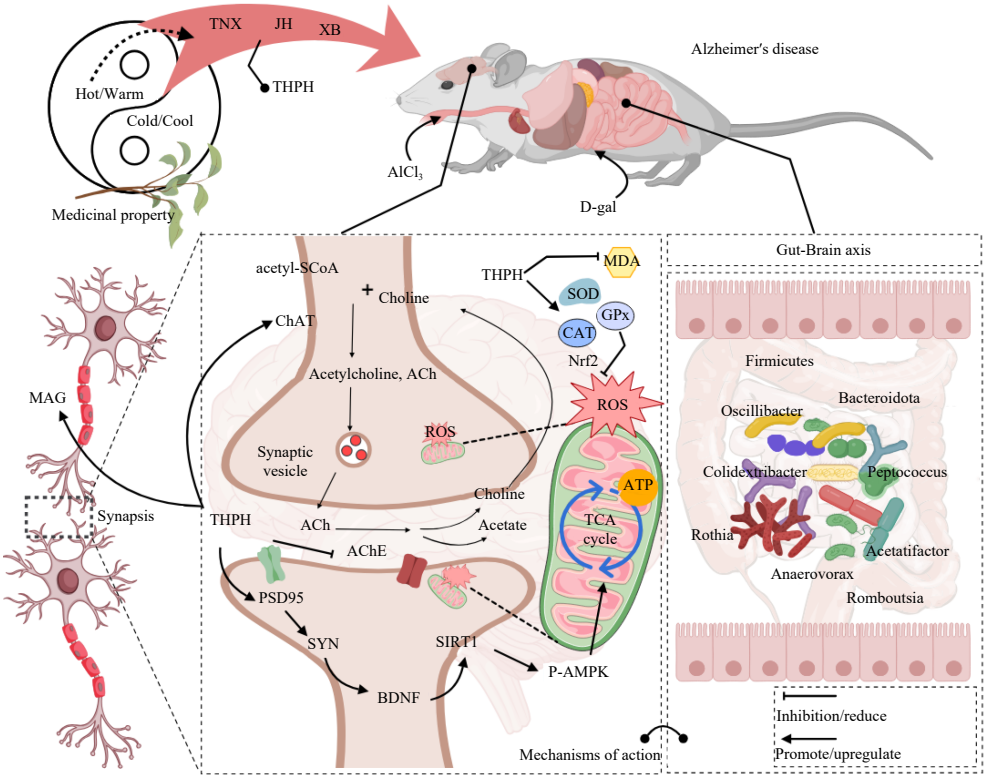


Fig. 9 Schematic diagram of the molecular signal regulation mechanism of THPH to promote neurological function improvement after AD.

ciated with AD.

AD, characterized by progressive memory decline and executive dysfunction, falls under the TCM classifications of "Dai Bing" (dementia) and "Jian Wang" (amnesia) [45]. The primary TCM pathological mechanisms involve kidney deficiency, brain-marrows consumption, phlegm-turbidity obstruction, and blood stasis stagnation, which are clinically categorized as "Xu Han Zheng" (deficiency-cold syndrome) or "Tan Yu Zheng" (phlegm-blood stasis syndrome). TCM posits that a decline in Yang leads to cerebral cold and mental dysfunction, resulting in amnesia; insufficient Yang impedes qi and blood circulation, causing phlegm and blood stasis to obstruct cerebral orifices. Patients with AD frequently exhibit lethargy, slow responses, and apathy, alongside cold manifestations such as cold limbs and poor appetite. Clinically, warm-natured herbs like *Acorus gramineus* [46], *Polygala tenuifolia* Willd. [47], and *Panax ginseng* C. A. Mey. [48] are employed to warm Yang-qi, rejuvenate the mind, replenish qi, and resolve phlegm. This study observed energy metabolism disorders in AD model rats, characterized by reduced biomarkers related to energy metabolism (e.g., isocitric acid, L-phenylalanine, sphinganine, thiamine, myo-inositol, D-galactose, and sucrose) and decreased phosphorylated AMPK levels, consistent with the hypometabolism, low heat production, and diminished energy utilization seen in deficiency-cold syndrome, which THPH effectively reversed. Furthermore, TCM asserts that AD lesions primarily affect the brain ("Sui Hai," the sea of brain marrow), relying on unobstructed collaterals to sustain mental function. Prolonged illness results in inadequate warming and nourishment of the brain marrow, leading to insufficiency, damage, and depletion, aligning with contemporary understanding of nerve myelin injury, demyelination, and remyelination disorders. Myelin injury, preceding classical protein abnormalities, facilitates plaque formation [49]; accumulated myelin debris promotes neuroinflammation, disrupts neurotransmitter balance, damages synapses, inhibits myelin regeneration and axonal growth, and ultimately leads to neural circuit failure [50]—reflecting the TCM pathogenesis of "Tan Zhuo Zu Qiao" (phlegm-turbidity blocking the brain orifices). THPH enhances synaptic count and upregulates synaptic-related proteins (BDNF, PSD95, SIRT1, MAG), thereby boosting synaptic plasticity and myelin integrity. This may lead to a reduction in brain debris accumulation and protection of the neural microenvironment. In conclusion, this study suggests that THPH can elevate basal metabolism, safeguard mitochondria, mitigate synaptic and myelin damage, rectify deficiency-cold pathology through energy metabolism regulation, provide myelin protection, and improve conditions associated with "Sui Han" (brain marrow cold) and "Tan Yu" (phlegm and blood stasis).

5. Conclusion

In conclusion, this study employed an integrated approach that combined data mining pharmacodynamics, network pharmacology, metabolomics, proteomics, and gut microbiota analysis to investigate the effects of THPH (warm TCMs of this study) and TCPH (cold TCMs of this study) on AD. The findings demonstrate that THPH exerts neuroprotective effects by alleviating cognitive and memory impairments induced by D-galactose and $AlCl_3$, showing superior neuroprotection compared to TCPH. The potential mechanisms underlying THPH's effects involve the enhancement of mature neuron populations, mitigation of neuropathological damage, reduction of oxidative stress, modulation of the cholinergic system, improvement of energy metabolism, restoration of synaptic function, and normalization of gut microbiota dysbiosis. This study provides a theoretical foundation for further promoting the integration of medicinal property-based approaches in clinical practice. However, other hot-acting and cold-acting herbs not included in this study may exhibit different therapeutic effects on AD. Further research and validation are necessary.

Funding

This work was supported by the Chief Scientist of Qi-Huang Project of National Traditional Chinese Medicine Inheritance and Innovation"One Hundred Million" Talent Project ([2021] No. 7), Qi-Huang Scholar of National Traditional Chinese Medicine Leading Talents Support Program ([2018] No. 284), National Famous Old Traditional Chinese Medicine Experts Inheritance Studio Construction Program of National Administration of TCM ([2022] No. 75), The Seventh Batch of National Famous Old Traditional Chinese Medicine Experts Experience Heritage Construction Program of National Administration of TCM ([2022] No. 76), and the Heilongjiang Touyan Innovation Team Program ([2019] No. 5).

Supplementary materials

Supplementary data associated with this article can be requested by sending E-mail to the corresponding authors.

Declaration of competing interest

There are no conflicts of interest to declare.

References

1 Wang YY, Sun YP, Yang BY, et al. Application of metabolomics and network analysis to reveal the ameliorating effect of four typical "hot" property herbs on hypothyroidism rats. *Front Pharmacol*. 2022;13:955905. https://doi.org/10.3389/fphar.2022.955905.
2 Wu JS, Luo Y, Deng DH, et al. Coptisine from *Coptis chinensis* exerts diverse beneficial properties: a concise review. *J Cell Mol Med*. 2019;23(12):7946-7960. https://doi.org/10.1111/jcmm.14725.
3 Wei GH, Fu XJ, Wang ZG. Multisolvent similarity measure of Chinese herbal medicine ingredients for cold–hot nature identification. *J Chem Inf Model*. 2019;59(12):5065-5073. https://doi.org/10.1021/acs.jcim.9b00682.
4 Wang YY, Sun YP, Yang BY, et al. Integrate metabolomics strategy and target prediction to reveal the ameliorate effect of four typical 'cold' property herbs on hyperthyroidism rats. *J Ethnopharmacol*. 2023;301:115772. https://doi.org/10.1016/j.jep.2022.115772.
5 Sultana OF, Bandaru M, Bushra MSTA, et al. Serotonin-mediated regulation of mitophagy in Alzheimer's disease: mechanistic insights and therapeutic potential. *Ageing Res Rev*. 2026;114:102957. https://doi.org/10.1016/j.arr.2025.102957.
6 Xu LF, Liu R, Qin YK, et al. Brain metabolism in Alzheimer's disease: biological mechanisms of exercise. *Transl Neurodegener*. 2023;12(1):33. https://doi.org/10.1186/s40035-023-00364-y.
7 Tang KS. The cellular and molecular processes associated with scopolamine-induced memory deficit: A model of Alzheimer's biomarkers. *Life Sci*. 2019;233:116695. https://doi.org/10.1016/j.lfs.2019.116695.
8 Zhang ML, Zhao X, Li WX, et al. Yin/Yang associated differential responses to *Psoralea corylifolia* Linn in rat models: an integrated metabolomics and transcriptomics study. *Chin Med*. 2023;18(1):102. https://doi.org/10.1186/s13020-023-00793-x.
9 Zhang M, Zhang X, Wei R, et al. Principles and strategies in cold/hot property studies of traditional Chinese medicine: an evolution from traditional theory to modern elucidation. *J Pharm Anal*. 2025;16(6):101455. https://doi.org/10.1016/j.jpha.2025.101455.
10 Luo YL, Zhou Y, Song MM, et al. Analyze the application and mechanism of Traditional Chinese Medicine in chronic urticaria based on data mining and network pharmacology. *Chin J Anal Chem*. 2025;53(4):100512. https://doi.org/10.1016/J.CJAC.2025.100512.
11 Chiroma SM, Mohd Moklas MA, Mat Taib CN, et al. D-galactose and aluminium chloride induced rat model with cognitive impairments. *Biomed Pharmacother*. 2018;103:1602-1608. https://doi.org/10.1016/j.biopha.2018.04.152.
12 Liu M, Zeng MN, Wang SC, et al. Thymidine and 2′-deoxyuridine reduce microglial activation and improve oxidative stress damage by modulating glycolytic metabolism on the $A\beta_{25-35}$-induced brain injury. *Arch Biochem Biophys*. 2022;729:109377. https://doi.org/10.1016/j.abb.2022.109377.
13 Ni HJ, Liu MQ, Cao MD, et al. Sinomenine regulates the cholinergic anti-inflammatory pathway to inhibit TLR4/NF-κB pathway and protect the homeostasis in brain and gut in scopolamine-induced Alzheimer's disease mice. *Biomed Pharmacother*. 2024;171:116190. https://doi.org/10.1016/j.biopha.2024.116190.
14 Khan T, Waseem R, Shahid M, et al. Recent advancement in therapeutic strategies for Alzheimer's disease: insights from clinical trials. *Ageing Res Rev*. 2023;92:102113. https://doi.org/10.1016/j.arr.2023.102113.
15 He ZJ, Li XQ, Wang Z, et al. Protective effects of luteolin against amyloid beta-

induced oxidative stress and mitochondrial impairments through peroxisome proliferator-activated receptor γ-dependent mechanism in Alzheimer's disease. *Redox Biol*. 2023;66:102848. https://doi.org/10.1016/j.redox.2023.102848.
16 Li DL, Cai CP, Liao YF, et al. Systems pharmacology approach uncovers the therapeutic mechanism of medicarpin against scopolamine-induced memory loss. *Phytomedicine*. 2021;91:153662. https://doi.org/10.1016/j.phymed.2021.153662.
17 Clarke JR, Ribeiro FC, Frozza RL, et al. Metabolic dysfunction in Alzheimer's disease: from basic neurobiology to clinical approaches. *J Alzheimers Dis*. 2018;64(s1):S405-S426. https://doi.org/10.3233/jad-179911.
18 Zocchi L, Sassone-Corsi P. SIRT1-mediated deacetylation of MeCP2 contributes to BDNF expression. *Epigenetics*. 2014;7(7):695-700. https://doi.org/10.4161/epi.20733.
19 Bélanger M, Allaman I, Magistretti PJ. Brain energy metabolism: focus on astrocyte-neuron metabolic cooperation. *Cell Metab*. 2011;14(6):724-738. https://doi.org/10.1016/j.cmet.2011.08.016.
20 Benaroya H. Brain energetics, mitochondria, and traumatic brain injury. *Rev Neurosci*. 2020;31(4):363-390. https://doi.org/10.1515/revneuro-2019-0086.
21 Gowda P, Reddy PH, Kumar S. Deregulated mitochondrial microRNAs in Alzheimer's disease: focus on synapse and mitochondria. *Ageing Res Rev*. 2022;73:101529. https://doi.org/10.1016/j.arr.2021.101529.
22 Zhao X, Fang JK, Li S, et al. Artemisinin attenuated hydrogen peroxide (H_2O_2)-induced oxidative injury in SH-SY5Y and hippocampal neurons *via* the activation of AMPK Pathway. *Int J Mol Sci*. 2019;20(11):2680. https://doi.org/10.3390/ijms20112680.
23 Theparambil SM, Kopach O, Braga A, et al. Adenosine signalling to astrocytes coordinates brain metabolism and function. *Nature*. 2024;632(8023):139-146. https://doi.org/10.1038/s41586-024-07611-w.
24 Duran-Aniotz C, Hetz C. Glucose metabolism: s sweet relief of Alzheimer's disease. *Curr Biol*. 2016;26(17):R806-R809. https://doi.org/10.1016/j.cub.2016.07.060.
25 Bekdash RA. The cholinergic system, the adrenergic system and the neuropathology of Alzheimer's disease. *Int J Mol Sci*. 2021;22(3):1273. https://doi.org/10.3390/ijms22031273.
26 Gu X, Wang XY. An overview of recent analysis and detection of acetylcholine. *Anal Biochem*. 2021;632:114381. https://doi.org/10.1016/j.ab.2021.114381.
27 Tabner BJ, El-Agnaf OMA, Turnbull S, et al. Hydrogen peroxide is generated during the very early stages of aggregation of the amyloid peptides implicated in Alzheimer disease and familial British dementia. *J Biol Chem*. 2005;280(43):35789-35792. https://doi.org/10.1074/jbc.C500238200.
28 Kowalska M, Piekut T, Prendecki M, et al. Mitochondrial and nuclear DNA oxidative damage in physiological and pathological aging. *DNA Cell Biol*. 2020;39(8):1410-1420. https://doi.org/10.1089/dna.2019.5347.
29 Dewanjee S, Chakraborty P, Bhattacharya H, et al. Altered glucose metabolism in Alzheimer's disease: role of mitochondrial dysfunction and oxidative stress. *Free Radic Biol Med*. 2022;193:134-157. https://doi.org/10.1016/j.freeradbiomed.2022.09.032.
30 Lachkar F, Ferré P, Foufelle F, et al. Dihydroceramides: their emerging physiological roles and functions in cancer and metabolic diseases. *Am J Physiol Endocrinol Metab*. 2021;320(1):E122-E130. https://doi.org/10.1152/ajpendo.00330.2020.
31 Hatanaka H, Hanyu H, Fukasawa R, et al. Differences in peripheral oxidative stress markers in Alzheimer's disease, vascular dementia and mixed dementia patients. *Geriatr Gerontol Int*. 2015;15(S1):53-58. https://doi.org/10.1111/ggi.12659.
32 Xia CR, Tian QY, Kong LY, et al. Metabolomics analysis for nitrite degradation by the metabolites of limosilactobacillus fermentum RC4. *Foods*. 2022;11(7):1009-1009. https://doi.org/10.3390/foods11071009.
33 Carvalho-Silva M, Gomes LM, de Prá SD-T, et al. Evidence of hippocampal astrogliosis and antioxidant imbalance after L-tyrosine chronic administration in rats. *Metab Brain Dis*. 2019;35(1):193-200. https://doi.org/10.1007/s11011-019-00511-3.
34 Lin CC, Yang CC, Chen YW, et al. Arachidonic acid induces ARE/Nrf2-dependent heme oxygenase-1 transcription in rat brain astrocytes. *Mol Neurobiol*. 2017;55(4):3328-3343. https://doi.org/10.1007/s12035-017-0590-7.
35 Cao XF, Guo HX, Dai YJ, et al. Excessive linoleic acid induces muscle oxidative stress through 5-lipoxygenase-dependent peroxidation. *Redox Biol*. 2024;71:103096. https://doi.org/10.1016/j.redox.2024.103096.
36 Liu Q, Wang SC, Ding K. Research advances in the treatment of Alzheimer's disease with polysaccharides from traditional Chinese medicine. *Chin J Nat Med*. 2017;15(9):641-652. https://doi.org/10.1016/s1875-5364(17)30093-6.
37 Zhou H, Yin XH, Zhang GQ, et al. Advancing nanomaterial-based strategies for Alzheimer's disease: a perspective. *JACS Au*. 2025;5(4):1519-1537. https://doi.org/10.1021/jacsau.5c00002.
38 Shi HS, Yu YH, Lin DH, et al. β-Glucan attenuates cognitive impairment *via* the gut-brain axis in diet-induced obese mice. *Microbiome*. 2020;8(1):143. https://doi.org/10.1186/s40168-020-00920-y.
39 Ren TY, Chen Z, Xie J, et al. Studies on the role of *Rosa roxburghii* Tratt quercetin in improving intestinal metabolism and the microbiome in mice with Alzheimer's disease. *J Funct Foods*. 2024;114:106046. https://doi.org/10.1016/j.jff.2024.106046.
40 Chen YY, Chen SY, Chang HY, et al. *Phyllanthus emblica* L. polysaccharides ameliorate colitis *via* microbiota modulation and dual inhibition of the RAGE/NF-κB and MAPKs signaling pathways in rats. *Int J Biol Macromol*. 2024;258:129043. https://doi.org/10.1016/j.ijbiomac.2023.129043.
41 Feng RB, Wang Q, Yu TT, et al. Quercetin ameliorates bone loss in OVX rats by modulating the intestinal flora-SCFAs-inflammatory signaling axis. *Int Immunopharmacol*. 2024;136:112341. https://doi.org/10.1016/j.intimp.2024.112341.
42 Hu ZM, Chu ZX, Ling XK, et al. Sinensetin from citrus peel alleviates DSS-induced inflammation by regulating gut microbiota and serum metabolism in mice. *Food Biosci*. 2024;62:105066. https://doi.org/10.1016/j.fbio.2024.105066.
43 Zhang Q, Wu GR, Shen SM, et al. *Dioscoreae persimilis* polysaccharide ameliorates DSS-induced ulcerative colitis in mice through modulation of microbiota composition. *JHIP*. 2023;4(2):157-165. https://doi.org/10.1016/j.jhip.2023.09.004.
44 Kang J, Li CQ, Gao XH, et al. Metformin inhibits tumor growth and affects intestinal flora in diabetic tumor-bearing mice. *Eur J Pharmacol*. 2021;912:174605. https://doi.org/10.1016/j.ejphar.2021.174605.
45 Hahn R. Treatment of neuropsychiatric symptoms in Alzheimer's disease with traditional Chinese medicine: an integrative medicine case report. *Adv Integr Med*. 2024;11(4):240-246. https://doi.org/10.1016/j.aimed.2024.08.008.
46 Xiong R, Liu HX, Zhang SP, et al. *Acorus tatarinowii* Schott attenuates Alzheimer's disease *via* neuronal ferroptosis inhibition: a synergistic network pharmacology and multi-omics profiling study. *J Ethnopharmacol*. 2026;356:120829. https://doi.org/10.1016/j.jep.2025.120829.
47 Garg A, Agrawal R, Deshmukh R. Pharmacology of polygala tenuifolia and its significance in traditional Chinese medicine. *Pharmacol Res Modern Chin Med*. 2024;10:100341. https://doi.org/10.1016/j.prmcm.2023.100341.
48 Hwang J, Keum M, Choe YM, et al. *Panax ginseng*: a modulator of amyloid, tau pathology, and cognitive function in Alzheimer's disease. *J Ginseng Res*. 2025;49(4):348-355. https://doi.org/10.1016/j.jgr.2025.03.011.
49 Maitre M, Jeltsch-David H, Okechukwu NG, et al. Myelin in Alzheimer's disease: culprit or bystander? *Acta Neuropathol Commun*. 2023;11(1): 56. https://doi.org/10.1186/s40478-023-01554-5.
50 Sen MK, Mahns DA, Coorssen JR, et al. The roles of microglia and astrocytes in phagocytosis and myelination: insights from the cuprizone model of multiple sclerosis. *Glia*. 2022;70(7):1215-1250. https://doi.org/10.1002/glia.24148.